



ORIGINAL RESEARCH ARTICLE

Microstructure and Wear Behavior of AlCoCrFeNiTi_{0.5} High Entropy Alloy Coating Prepared by Electron Beam Cladding on Ti-6Al-4V Substrate

Yulong Li, Bin Tang, Haoyue Wu, Min Lei, Xuwen Li, Hua Ouyang, and Wenqin Wang

Submitted: 14 January 2023 / Revised: 17 May 2023 / Accepted: 3 June 2023

AlCoCrFeNiTi_{0.5} high entropy alloy (HEA) coating with high hardness and excellent wear resistance was deposited on TC4 surface by electron beam cladding, and the process parameters, microstructure and properties of the coating were studied. The analysis shows that the microstructure of HEA coating is composed of dendritic (DR) and interdendritic (IR) phases. The IR phase, which is mainly composed of Fe and Cr, is confirmed to be BCC solid solution, while the DR phase is FCC solid solution with AlNi₂Ti (or AlCo₂Ti) structure. The grain orientation of the HEA coating is random, without obvious texture. Hardness gradually decreases from the upper part area of the HEA coating to the inner of the TC4 substrate. The hardness curve in the HEA coating region has some fluctuations, but the fluctuations are small, indicating a homogeneous microstructure. The average hardness of the HEA coating is 796.18 HV_{0.2}, which is about 2.6 times that of the TC4 substrate. The HEA coating exhibits a higher coefficient of friction (COF) compared to the TC4 substrate. The average COF of HEA coating and TC4 substrate in the stable stage are 0.57 and 0.48, respectively. Wear loss of the HEA coating is 0.0657 mm³, about one tenth of that of TC4 substrate (0.6112 mm³). The hardness of the HEA coating is high, no obvious furrow is found, and its wear mechanism is considered to be a mixture of adhesive wear and oxidation wear.

Keywords AlCoCrFeNiTi_{0.5}, electron beam cladding, high entropy alloy, microhardness, Ti-6Al-4V, wear

1. Introduction

High entropy alloy (HEA) is a new type of alloy, which is usually defined as an alloy with multiple metal elements (five or more), and the atomic fraction ratio of each other is between 5 and 35%. HEA has excellent mechanical properties (Ref 1-3), such as high hardness (Ref 4, 5), good wear resistance (Ref 6-8), excellent corrosion resistance (Ref 9, 10) and high temperature oxidation resistance (Ref 11-13). Recently, the AlCoCrFeNiTi_x alloy system is one of the hot research foci. Research has shown that the appropriate amount of Ti can cause lattice distortion in HEA coating and generate large distortion energy, thus improving the mechanical properties

(Ref 14); however, the brittleness of HEA increases with increasing Ti content. AlCoCrFeNiTi_{0.5} HEA has good wear resistance, high strength, and high hardness. Kong et al. (Ref 15) successfully prepared AlCoCrFeNiTi_{0.5} HEA. After remelting and annealing treatment, the mean microhardness of the HEA was increased by 8.2 and 26%, respectively, and the wear loss was significantly reduced, showing better wear resistance. Zhou et al. (Ref 16) successfully prepared AlCoCrFeNiTi_x HEA and found that AlCoCrFeNiTi_{0.5} HEA has a uniform microstructure and excellent comprehensive mechanical properties. Zhou et al. (Ref 17) prepared AlCoCrFeNiTi_{0.5} HEA using copper mold suction casting after arc melting and studied its microstructure and room temperature compression properties. The result shows that AlCoCrFeNiTi_{0.5} HEA has excellent room temperature mechanical properties, with yield strength, fracture strength, and plastic deformation reaching 2.26 GPa, 3.14 GPa, and 23.3%, respectively, surpassing most high-strength alloys, such as bulk amorphous alloys. Zeng et al. (Ref 18) studied the high-temperature oxidation resistance of AlCoCrFeNiTi_{0.5} HEA at 600 °C. The results indicate that the HEA has better oxidation resistance than the TC4, with a lower oxidation rate (about one tenth of the TC4) and a smaller oxidation scale (about one fifth of the TC4). Cui et al. (Ref 19) investigated the hardness and oxidation resistance of AlCoCrFeNiTi_{0.5} HEA. The result shows that the hardness of AlCoCrFeNiTi_{0.5} HEA is 634 HV, about 2.1 times that of TC4. In the oxidation experiment at 700 °C, the weight gain of the HEA was 0.23 mg/cm² and that of TC4 was 5.87 mg/cm², indicating that the HEA showed better oxidation resistance. Overall, AlCoCrFeNiTi_{0.5} HEA has more outstanding compre-

Yulong Li, Bin Tang, Min Lei, and Wenqin Wang Key Lab for Robot & Welding Automation of Jiangxi Province, School of Advanced Manufacturing, Nanchang University, Nanchang 330031, China; **Haoyue Wu**, Department of Physics, School of Physics and Materials Science, Nanchang University, Nanchang 330031, China; and **Xuwen Li, Hua Ouyang**, The Engineering Training Center of Nanchang University, Mechanical & Electrical Engineering School, Nanchang University, Nanchang 330031, China. Contact e-mails: lixuwen@ncu.edu.cn and wangwenqin@ncu.edu.cn.

hensive mechanical properties, good wear resistance, and excellent high-temperature oxidation resistance in the explored HEA system. Moreover, there is no significant difference in segregation coefficients among the components of AlCoCrFeNiTi_{0.5} HEA, which can make the internal composition of AlCoCrFeNiTi_{0.5} HEA uniform and reduce the occurrence of cracks and other defects (Ref 20). Due to the excellent performance of AlCoCrFeNiTi_{0.5} HEA, this HEA has been selected in this study and some other research work.

HEA can be used as a coating material for surface modification to improve the surface properties of titanium alloys. The surface modification technology acts on the surface of the substrate and has little influence on the internal structure and properties of the substrate, so it can maintain good comprehensive properties. The traditional surface modification technologies mainly include electroless plating (Ref 21-23), thermal spraying (Ref 24-26), laser processing (Ref 27-30), arc cladding (Ref 31, 32), *etc.* Dai et al. (Ref 33) successfully prepared CuCoNi alloy coating using electroless plating, proposed a new HEA coating design method, and applied it on the surface of highly conductive copper sheet. Vallimanan et al. (Ref 34) successfully synthesized AlCoCrMoNi HEA coating on SS316L substrate by thermal spraying process, compared with the conventional NiCrSiB corrosion resistant coating, the HEA coating also has excellent corrosion resistance. Li et al. (Ref 35) successfully prepared an amorphous TiNiSiCrCoAl HEA coating using laser cladding. Compared with the TC4 substrate, the oxidation resistance of the HEA coating increased by 11, 28, 41, and 65 times at different laser scanning speeds under oxidation at 800 °C for 48 h. Liu et al. (Ref 36) successfully prepared the CoCrFeNiW_x HEA coating using laser cladding, they found that appropriate W addition can reduce defects, increase the microhardness, and enhance the high-temperature performance. Fan et al. (Ref 32) successfully prepared AlCoCrFeNi HEA coating using arc cladding and the results show that the histomorphology of HEA coating changes from disordered granular to dendritic when the Fe content increases to a certain value.

In current research, laser cladding is a commonly used process to prepare HEA coating, while electron beam cladding has been studied to a moderate extent. Compared with laser cladding technology, electron beam cladding has higher energy utilization rate, faster processing speed and better power parameter control. What it's more, the electron beam cladding experiment is conducted in a vacuum chamber, it can effectively avoid the oxidation of the substrate material due to exposure to air during the cladding process, and will not pollute the environment due to the sublimation of the powder material (Ref 37). Electron beam cladding of titanium alloy in vacuum can also prevent hydrogen evolution embrittlement (Ref 38). The electron beam cladding technology uses the electron beam with high energy density as the heat source. Pre-coated alloy powders with special physical and chemical properties are coated on the substrate surface with a thickness of a few millimeters by thermal spraying, adhesion, pressing and other processing methods. Then, the surface of the coating material is irradiated by the electron beam with high energy density. The treated coating melts instantaneously and forms a new alloy layer by melting together with the substrate, to obtain the microstructure and properties suitable to the design requirements, this makes up for the lack of surface properties of the material workpiece. Yu et al. (Ref 39) successfully

prepared AlCrTiNbMo HEA coating using electron beam cladding and carried out hardness measurement and friction and wear experiments. After analyzing the results of hardness measurement experiments, it can be concluded that hardness gradually decreases from the coating to the substrate, so the coating has been proved to have higher hardness. In the analysis of the wear mechanism, the coating shows the wear characteristics of micro-cutting. After the wear experiment, the wear quality of the coating is calculated to be about one eighth of the substrate. Yu et al. (Ref 40) prepared Mo₂₀Nb₂₀Co₂₀Cr₂₀ (Ti₈Al₈Si₄) refractory HEA coating by electron beam cladding under different cladding currents. In this experiment, with the increase in cladding current, Mo and other solid solution elements cause a lattice distortion effect in HEA coating, which makes the dislocation movement more difficult, which makes the deformation of HEA coating during wear requiring more energy, and ultimately the wear resistance increases significantly. As the current continues to increase, heat dissipation in the direction of the coating increases, resulting in coarser microstructure, reduced hardness and poor wear resistance of HEA coating. Ruktuev et al. (Ref 41) successfully prepared CoCrFeNi_x HEA coating (where X=Al, Cu, or Mn) on the surface of low-carbon steel using electron beam cladding. The result indicates that the hardness of CoCrFeNiCu and CoCrFeNiMn HEA coating is 190 and 186 HV, respectively. The hardness of CoCrFeNiAl HEA coating is 570 HV, 3.4 times higher than that of low-carbon steel. In the high-temperature oxidation experiment at 850 °C, the total mass gains of CoCrFeNiCu, CoCrFeNiMn, CoCrFeAl HEA coating and the substrate were 2.29, 2.04, 0.60, and, 41.01 mg/cm², respectively. The CoCrFeNiX HEA coating shows much better oxidation resistance.

Different from the above studies, this paper proposes for the first time to prepare AlCoCrFeNiTi_{0.5} HEA coating by electron beam cladding technology. Vacuum electron beam heating has the characteristics of high efficiency, rapid heating, rapid cooling, low dilution, and low porosity (Ref 42), so it is chosen as the heating source to manufacture the AlCoCrFeNiTi_{0.5} HEA coating on the surface of TC4. The internal structure of the electron beam cladding coating is uniform, with fewer cracks, pores or other defects than the coating obtained using other heating method. This not only enriches the preparation process of AlCoCrFeNiTi_{0.5} HEA coating, but also has important reference significance for future surface modification research and production application of titanium alloy. The microstructure, microhardness and wear behavior of the coating were studied by x-ray diffraction (XRD, D8 Advance), scanning electron microscopy (SEM, FEI Quanta 200FEG), energy dispersive spectroscopy (EDS), electron backscatter diffraction (EBSD, ZEISS SIGMA 300vp), microhardness test and friction and wear test.

2. Materials and Methods

A TC4 plate of 50×50×4 mm size was used as the base. The oxide on the surface of TC4 was removed by sandpaper, and then the impurities on the surface of the TC4 plate were removed by the ultrasonic cleaner. Pure Al, Co, Cr, Fe, Ni, and Ti powders (>99.5wt.%) were used as the coating materials, and the size of the powders ranged from 48 μm to 75 μm, which were mixed by planetary ball milling in argon gas for 2 h with a

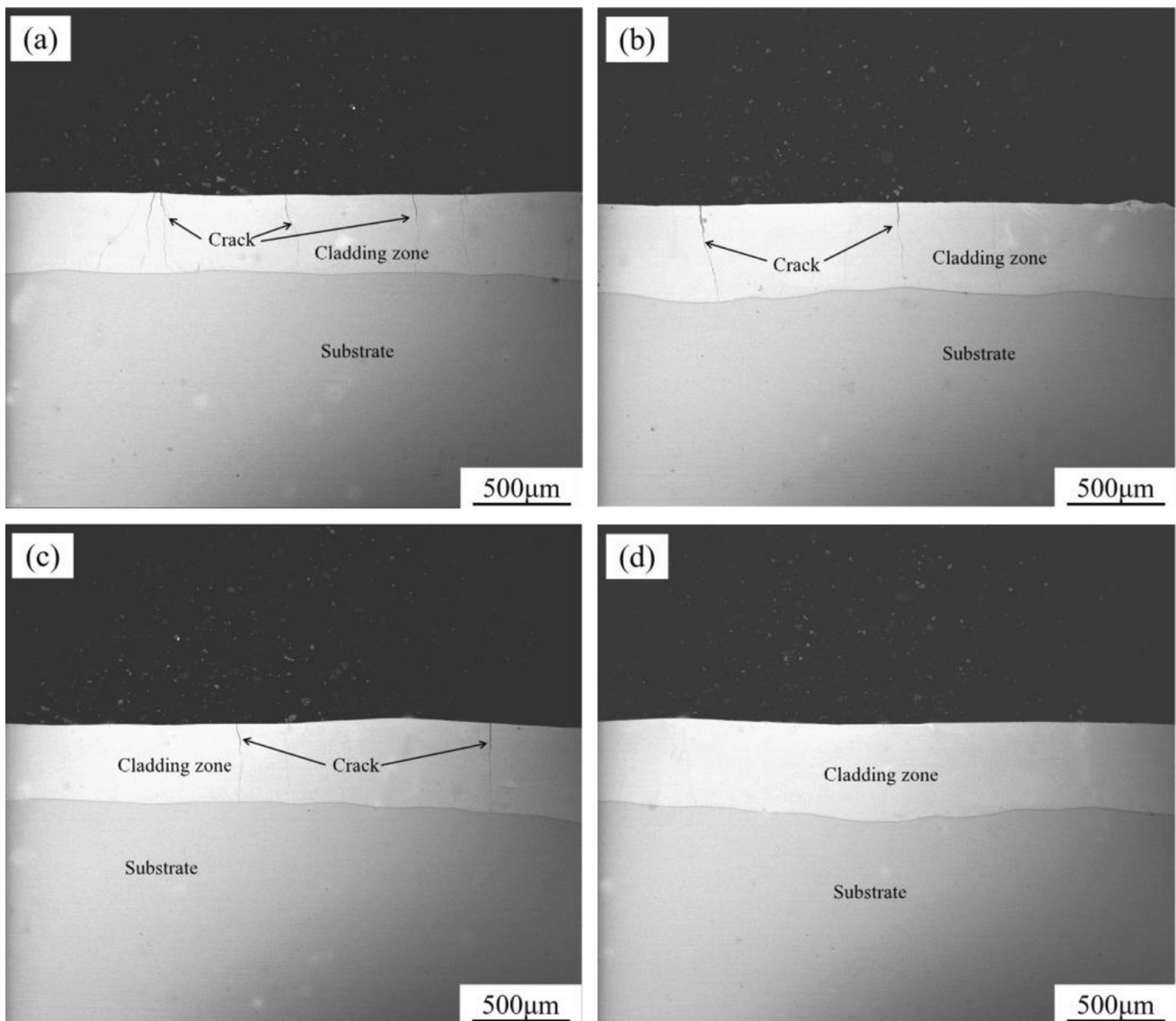


Fig. 1 Microstructure of the cladding layer of different current: (a) 16 mA, (b) 18 mA, (c) 20 mA, and (d) 22 mA

ball power ratio of 3:1 and a speed of 300 r/min. The experiments were performed using a Thdw-7 electron beam welder with electron beam melting parameters of high voltage 65 kV and the welding current was set as 16 mA, 18 mA, 20 mA and 22 mA, respectively. The electron beam scanning time was 4 s and the vacuum level was 5×10^{-2} Pa.

For the samples with optimal electron beam parameters, the TC4 substrate with cladding layer was cut into several cuboid samples of $10 \times 10 \times 4$ mm by an electric spark cutting machine. The sample was ground to 2000#, polished, and then etched in the solution (HF:HNO₃:H₂O=1:3:50 in volume) for 20 s to obtain the SEM sample to be tested. The XRD samples were also cut from the cladded TC4 with the size of $10 \times 10 \times 4$ mm. The cladded surface was ground flat and cleaned with acetone, alcohol and distilled water, and then the XRD test can be conducted. The microstructure of the coating was analyzed by XRD and SEM to observe whether the coating was well formed and to analyze the phase composition. The sample was

sanded to 2000# and mechanically polished, then plasma polishes were used to remove surface residual stress. The middle structure of the HEA coating is uniform, free from cracks and other obvious defects, so this area was selected for EBSD sampling and testing. The test was performed using the Oxford HKL Channel 5 software package. The sample tilt was 70°, the working distance was 12-15 mm, the working voltage was 20 kV, and the beam spot was 6. EBSD and EDS were used to analyze the grain boundary angles, grain distribution, and elemental composition of the coating. The microhardness tester (HV-1000) was used to measure the hardness of the sample five times at each position under a load of 100 g and a holding time of 20 s. A maximum value and a minimum value were removed, and the average of the remaining three values was taken. The wear behavior of the coating and TC4 substrate on Al₂O₃ balls (ϕ 6 mm) was tested using a multifunctional friction and wear tester (Bruker) under a load of 5 N, a linear speed of 20 mm/s, and a friction time of 30 min.

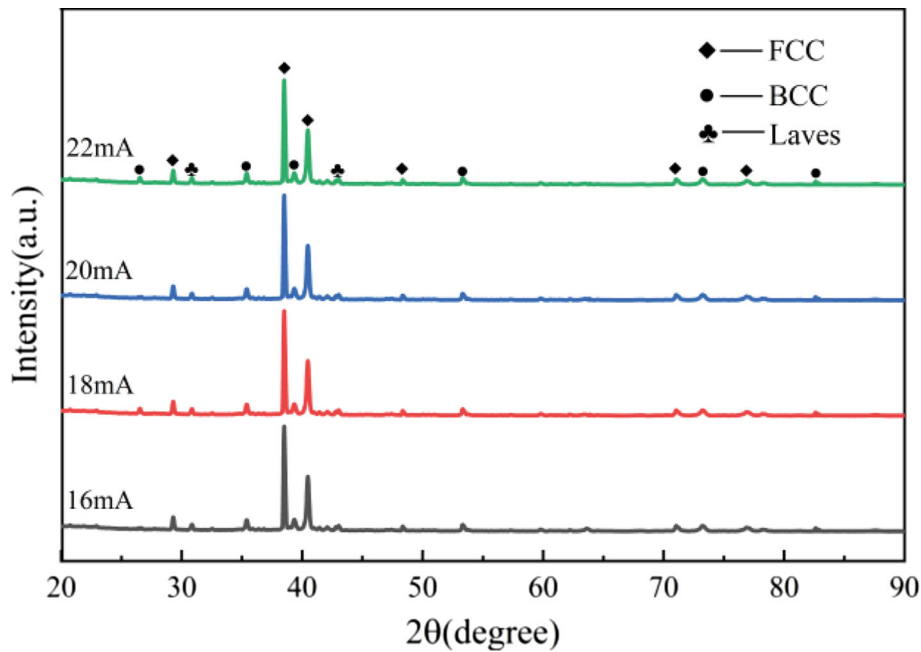


Fig. 2 XRD patterns of AlCoCrFeNiTi_{0.5} coating

2.1 Optimization of Electron Beam Cladding Parameters

Under different electron beam cladding parameters, the forming effect and hardness of the cladding layer have great differences. The right parameters can make the cladding layer well formed and free from defects such as cracks. As the experimental parameters are changed, the dilution ratio of Ti will also change, resulting in great changes in the hardness of the cladding layer under different parameters. The main factors affecting the effect of the cladding layer forming are the input power and scanning time of electron beam. The input power is mainly related to the acceleration voltage and welding current of the electron beam cladding parameters. Therefore, the controlled variable method was used to keep the acceleration voltage and scan time constant, and welding currents of 16, 18, 20, and 22 mA were used in the experiments.

Figure 1(a), (b), (c), and (d) shows the microstructure of the cladding layer under the welding current parameters of 16-22 mA. In Fig. 1(b), cracks and other defects can be observed. At low welding current, the HEA coating and TC4 substrate are not completely melted, the melt pool area is small, the outward diffusion range is not very large, and the mobility is poor, making the HEA coating structure uneven, resulting in cracks and other defects. With the increase in welding current, cracks and other defects in Fig. 1(b), (c), and (d) are less and less. In Fig. 1(d), the electron beam cladding layer has no crack and hole defects, and is well formed and bonded with the TC4 substrate. Therefore, 22 mA welding current is used as the optimal current parameter for the electron beam cladding experiment. Relatively speaking, with the increase in welding current, the higher input energy makes the surface of the coating more flatter, the coating and the TC4 substrate completely melt, and fully fuse, resulting in a larger melt pool, and the temperature in the coating area is getting higher and

higher, with large fluctuations, and the temperature difference with the TC4 substrate is getting larger and larger, and the enhancement of the heat dissipation ability of the molten pool to the TC4 substrate, leading to a more uniform microstructure of the HEA coating, better molding effect, and more refined grain structure. However, when the welding current exceeds 22 mA, the surface of the coating will gradually collapse under a higher welding current.

3. Results and Discussion

3.1 XRD Analysis

Figure 2 shows the XRD patterns of the AlCoCrFeNiTi_{0.5} HEA coating prepared under different electron beam welding currents. From Fig. 2, it is clear that the HEA coating mainly consists of FCC and BCC phases. The results show that under different welding current parameters, the main characteristic peaks of the HEA coating remain essentially unchanged, with only a slight change in the intensity of the peaks. This proves that the types of phases are essentially the same when the welding current is gradually increased within a certain range. By comparing the PDF cards, it can be concluded that the diffraction peak of FCC phase is consistent with AlNi₂Ti or AlCo₂Ti. The BCC phase is consistent with Fe-Cr phase. In addition, Laves phases are intermetallic compounds that have a stoichiometry of AB₂ and are often formed when the atomic size ratio is between 1.05 and 1.67. In the HEA coating, there are minor Laves phases (Fe₂Ti) presented along with the BCC phase and FCC phase as a matrix. The formation of compounds in HEA coating is mainly due to two reasons: (i) a large negative ΔH_{mix} promotes the formation of both short-range-

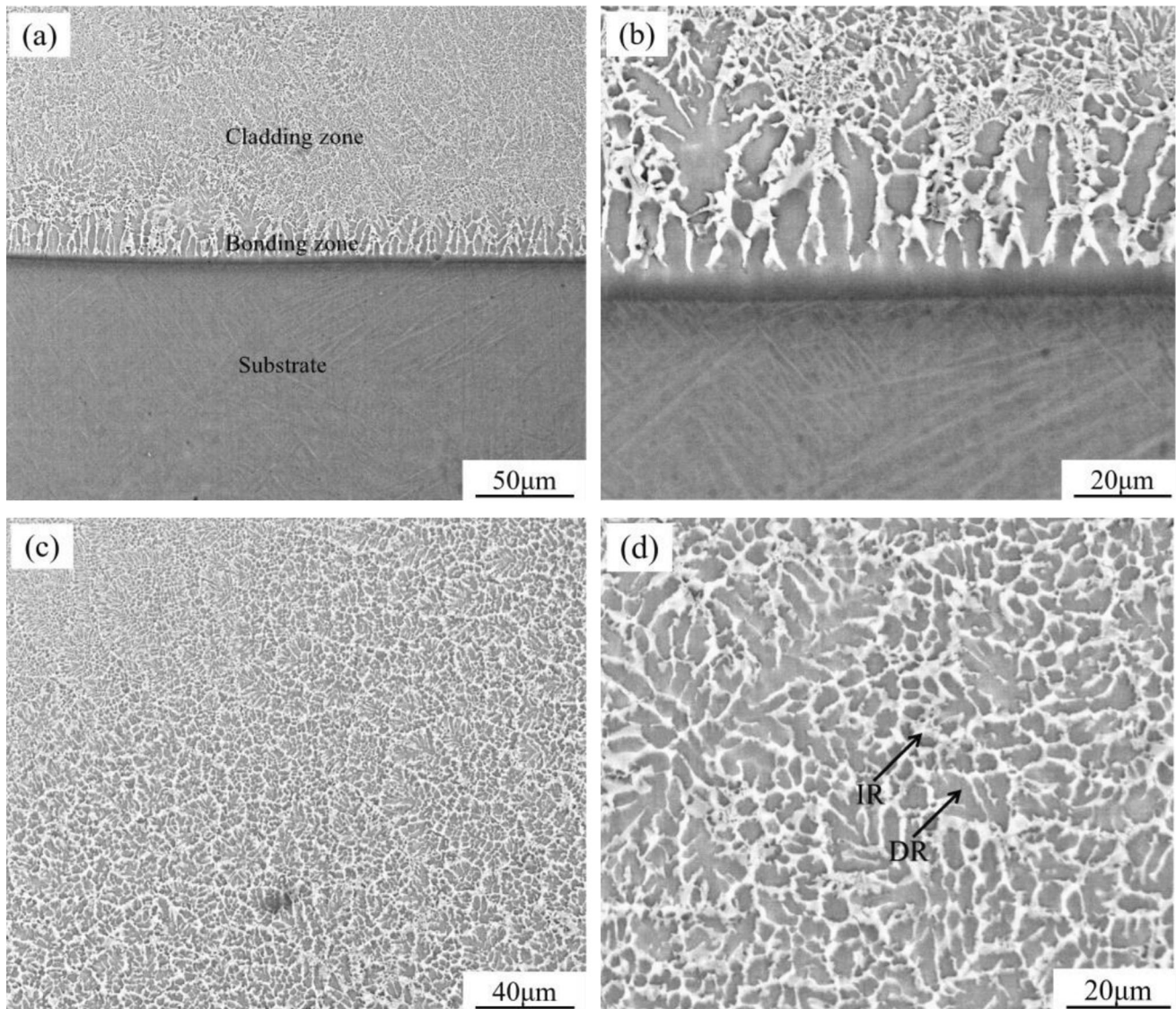


Fig. 3 Microstructure morphologies of AlCoCrFeNiTi_{0.5} HEA coating: (a) macroscopic feature; (b) bonding zone; (c) cladding zone; (d) enlarged view of cladding zone in Fig. (c)

Table 1 The chemical compositions of AlCoCrFeNiTi_{0.5} powders (%)

Element	Al	Co	Cr	Fe	Ni	Ti
Atomic fraction	18.18	18.18	18.18	18.18	18.18	9.09
Mass fraction	9.77	21.34	18.83	20.22	21.26	8.59

Table 2 EDS results of AlCoCrFeNiTi_{0.5} HEA coating (at.%)

Position/Element	Al	Co	Cr	Fe	Ni	Ti
DR	21.23	22.12	6.11	8.39	21.18	20.97
IR	1.59	5.62	45.92	35.49	4.79	6.59

ordered atomic clusters and long-range-ordered intermetallic compounds (Ref 43); (ii) contamination of grinding media and process control agent (Ref 44).

3.2 Microstructure of AlCoCrFeNiTi_{0.5} HEA Coating

Figure 3 shows the typical microstructure of AlCoCrFeNiTi_{0.5} HEA coating. From Fig. 3(a), (b), and (c), the macro feature, bonding area and cladding area of the HEA coating are shown, respectively. There are two microstructures in the cladding zone, namely DR and IR structures. It can be concluded that the coating has good internal molding, uniform structure, no cracks, holes and other defects, and a smooth surface. In addition, there is a smooth gray bright band in the bonding area, which indicates that the TC4 substrate and the HEA coating have good metallurgical bonding. There are plane crystals with a certain thickness above the bonding zone and columnar crystals growing perpendicular to the interface above the plane crystals (Table 1).

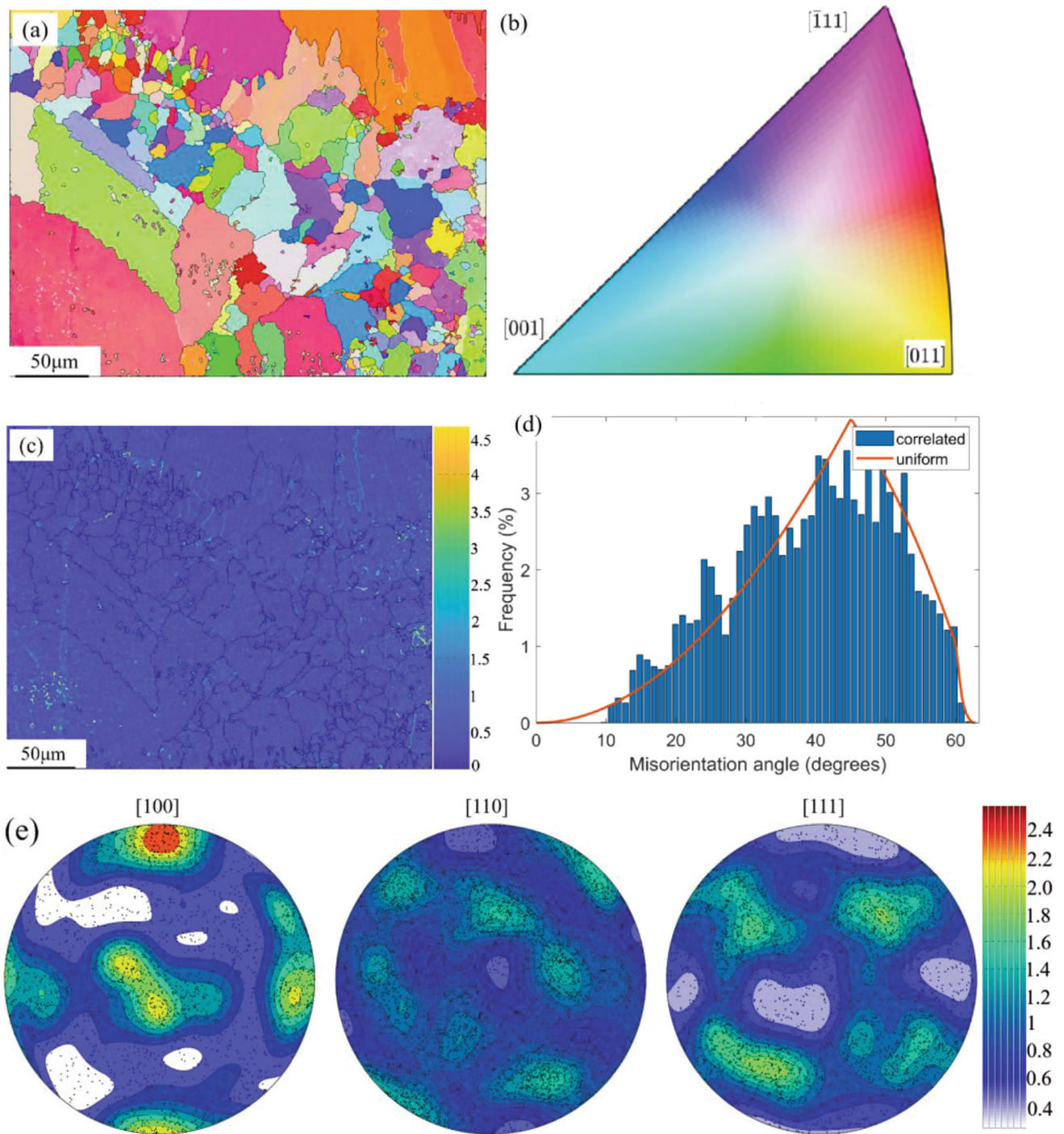


Fig. 4 (a) EBSD result of AlCoCrFeNiTi_{0.5} HEA coating; (b) IPF; (c) KAM diagram; (d) misorientation angle distribution histograms; (e) PF

From Fig. 3(c), the HEA coating consists of DR and IR phases, and Table 2 shows the composition of the coating. According to the XRD results, the analysis shows that IR phase is mainly composed of Fe and Cr elements, corresponding to the BCC phase. Moreover, the atomic contents of Al, Co, Ni, and Ti elements are basically the same, about 21%; therefore, DR phase mainly composed of Al, Co, and Ni is an equimolar FCC phase with AlNi₂Ti (or AlCo₂Ti) structure.

Figure 4(a), (b), (c), and (d) shows the EBSD image of the electron beam cladding layer. In Fig. 4(a), the cladding layer is

composed of some fine grains, a small number of columnar grains and massive grains, and the grain orientation is random. Figure 4(b) and (e) shows the pole figure (PF) and inverse pole figure (IPF), respectively. The extreme values of directional density of PF and IPF are 6.13 and 2.51, respectively. The lower value can confirm that the grain orientation is random. In Fig. 4(c), the local lattice distortion in the cladding area was analyzed using the kernel average misorientation (KAM). The KAM results can reflect the strain size inside the alloy, and its numerical value is positively correlated with the dislocation

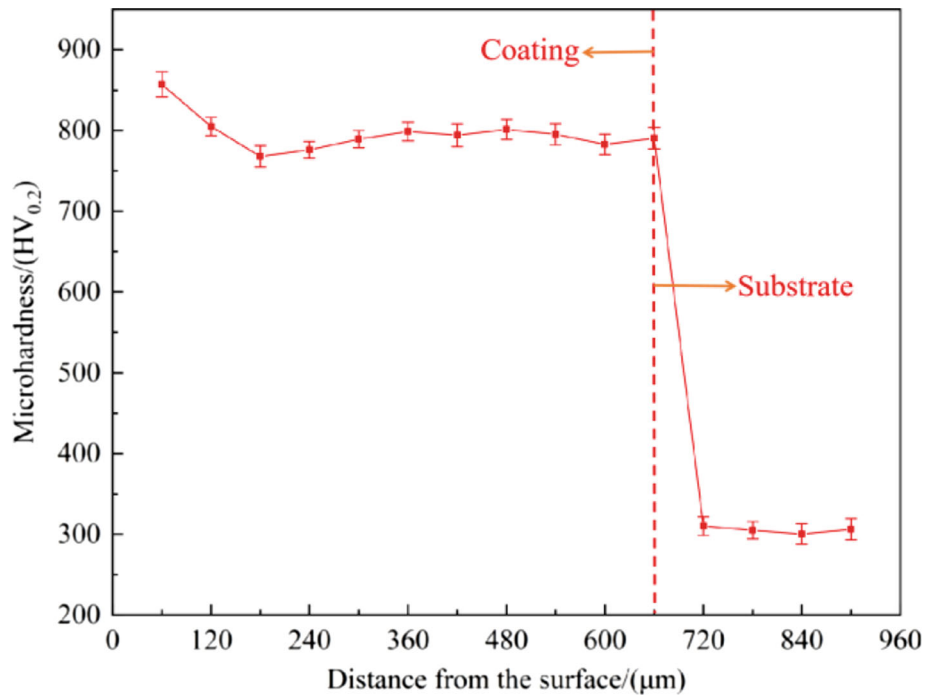


Fig. 5 Microhardness distribution in the cross section of the AlCoCrFeNiTi_{0.5} coating

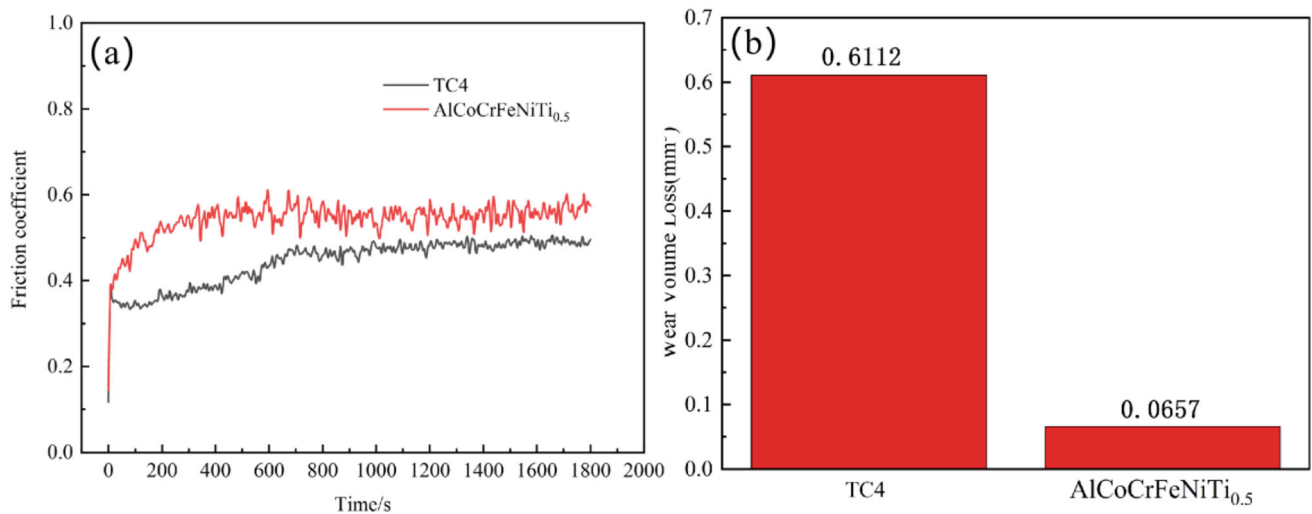


Fig. 6 (a) Friction coefficient-time curves of TC4 substrate and AlCoCrFeNiTi_{0.5} coating; (b) Wear volume loss of TC4 substrate and AlCoCrFeNiTi_{0.5} coating

density. The darker the color in the KAM diagram indicates the higher the dislocation density in this area (Ref 45). The green area in the KAM diagram indicates that there is a difference in grain orientation, which is confirmed to be the stress field caused by dislocation (Ref 46, 47). From the KAM diagram, it can be seen that there are few green areas, so it can be inferred that the stress between grains is not high, and cracks and other defects will not form in the cladding layer. In Fig. 4(d), the grain boundary distribution of the cladding layer is mainly composed of high-angle grain boundaries (HAGBs) ($\theta > 15^\circ$) composition. High angle grain boundary has very high grain boundary energy, which can make different elements fully diffuse with each other. After diffusion, the energy of grain

boundary decreases gradually and the grain boundary reaches a stable state.

3.3 Hardness Test

Figure 5 shows the microhardness of the cross section of the AlCoCrFeNiTi_{0.5} HEA coating. In Fig. 5, the microhardness curves generally show a decreasing trend, with some fluctuations in the HEA coating region, but the fluctuations are relatively small, which indicates a homogeneous microstructure. The fluctuation is because that electron beam cladding has the characteristics of rapid heating, melting, and solidifying, which can form a dense and uniform metallurgical layer with excellent performance, resulting in a relatively uniform distri-

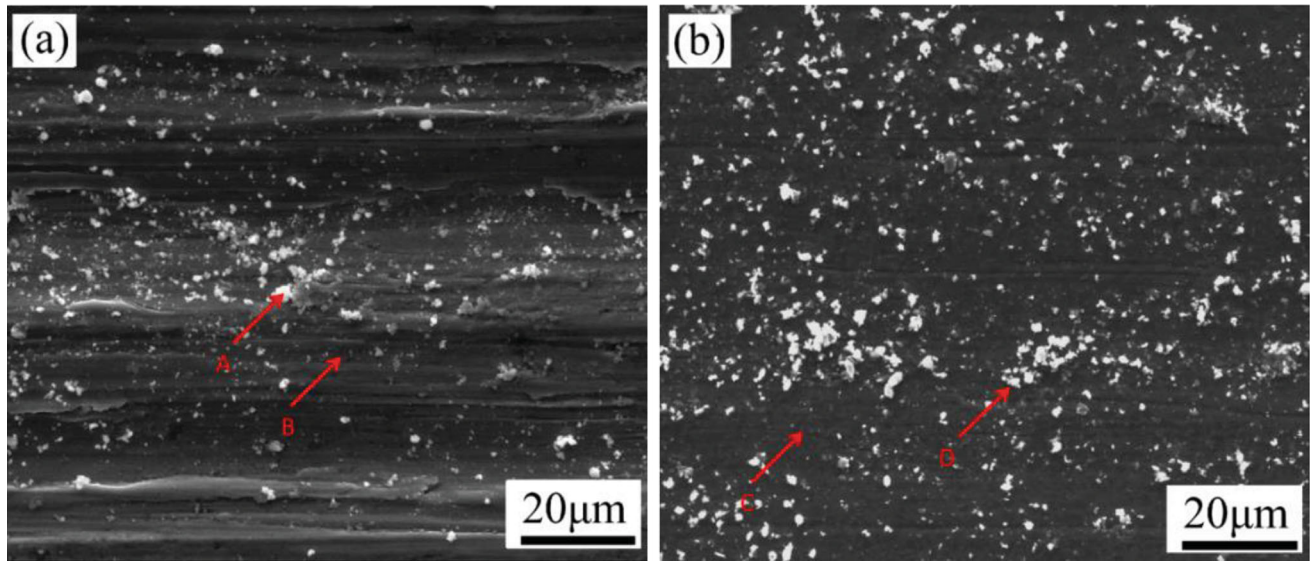


Fig. 7 Worn surface of (a) TC4 substrate and (b) AlCoCrFeNiTi_{0.5} coating

Table 3 EDS results of different regions in Fig. 7 (at.%)

Position/Element	Al	Co	Cr	Fe	Ni	Ti	V	O
A	10.25	41.10	2.24	46.41
B	9.38	54.92	3.49	32.21
C	12.65	2.23	3.11	9.53	18.23	2.99	0.03	51.23
D	9.77	2.21	2.45	10.21	14.32	2.92	...	58.12

bution of hardness inside the HEA coating. Hardness reaches the maximum in the HEA coating area and the minimum in the TC4 substrate, and hardness gradually decreases from the coating to the TC4 substrate. The average microhardness of the AlCoCrFeNiTi_{0.5} HEA coating is calculated to be 796.18 HV_{0.2}, which is approximately 2.6 times that of the TC4 substrate (305.6 HV_{0.2}). The larger radius of the Ti atoms occupying the lattice node positions leads to lattice distortion in HEA and generates larger distortion energy. The increase in deformation energy will promote the appearance of hard and amorphous phases in HEA, which will lead to solid solution strengthening of HEA, thus significantly improving the hardness. However, the appearance of hard phases will reduce the plasticity of HEA. Cr can optimize the mechanical properties of HEA, resulting in a certain degree of improvement in both strength and hardness. The addition of Cr to HEA will result in the appearance of BCC phase structure in HEA, which will increase the hardness, but the appearance of BCC phase will make HEA hard and brittle, and reduce the plasticity of HEA.

3.4 Wear Investigations

Figure 6(a) shows the COF curve of HEA coating and TC4 substrate at room temperature at 2 Hz frequency. It is obvious that the COF curve first enters a rapid upward phase and then enters a relatively stable state. When the COF curve reaches a relatively stable state, compared with TC4 substrate, HEA coating shows higher average COF, and their average COF is 0.48 and 0.57, respectively. There are two stages of the wear process, initial wear and stable wear, and the COF becomes

stable in about 700 s. In the stable wear stage, the COF of HEA coating fluctuates slightly, and the fluctuation is greater than that of the TC4 substrate, which is due to the smaller contact area between the friction pairs under low load conditions. At this time, the slight protrusion of the material surface causes the fluctuation of the COF curve. The calculated wear of the TC4 substrate and HEA coating is shown in Fig. 6(b). According to Fig. 6(b), the wear amount of the HEA coating is 0.0657 mm³, which is about one-tenth of the wear amount of the TC4 substrate (0.6112 mm³).

Figure 7(a) and (b) shows the wear surfaces of the TC4 substrate and AlCoCrFeNiTi_{0.5} coating, respectively. Since the hardness of the TC4 substrate is relatively low, its surface is severely worn and has obvious plastic deformation, and a large amount of debris is accumulated near the wear marks. Also, according to the analysis of the EDS results in Table 3, the oxygen content is high at points A and B, especially at location A (up to 46.41 at.%). Therefore, the TC4 substrate shows abrasive wear and oxidative wear characteristics (Ref 18). In Fig. 7(b), the coating exhibits adhesive wear and oxidative wear characteristics. The coating surface is slightly worn and accompanied by a certain degree of deformation, including flaky flaking debris and white particle binders. This is due to the micro-convex shearing and fracture of the adhering micro-bumps against each other during the wear process as the bumps above the specimen come into contact with the grinding balls and move relative to each other under a certain normal load, resulting in flaking. Because the coating hardness is high, no obvious plow grooves are observed. Instead, some smooth

areas (such as position C) and surface flaking (such as position D) are observed. In addition, the EDS results for positions C and D also show extremely high oxygen content of 51.23 and 58.12 at.%, respectively.

4. Conclusions

AlCoCrFeNiTi_{0.5} HEA coating was prepared on the TC4 surface using electron beam cladding method.

The optimal electron beam cladding parameters are obtained: the acceleration voltage is 65 kV, the welding beam current is 22 mA, and the electron beam scanning time is 4 s.

The HEA coating consists of DR and IR phases. IR phase is mainly composed of Fe and Cr elements, corresponding to the BCC phase. In addition, DR phase mainly composed of Al, Co and Ni is an equimolar FCC phase with AlNi₂Ti (or AlCo₂Ti) structure.

The average microhardness of AlCoCrFeNiTi_{0.5} HEA coating is tested to be 796.18 HV_{0.2}, which is about 2.6 times that of the TC4 substrate (305.6 HV_{0.2}).

The average COF of the HEA coating is 0.57, and the wear amount of the HEA coating is 0.0657 mm³, which is about one tenth of the TC4 substrate (0.6112 mm³).

Acknowledgments

This work was sponsored by the National Natural Science Foundation of China (52065043), the Central Guidance on Local: Construction of regional innovation system-Cross Regional R & D cooperation projects (20221ZDH04054), Technology Innovation High Level Talent Project of Double Thousand Plan of Jiangxi Province (jxsq2019201048), Natural Science Foundation of Chongqing (CSTB2022NSCQ-MSX1346).

Data Availability

Data will be made available on request.

Conflict of interest The authors declare that they have no known competing financial interests or personal relationships that could have appeared to influence the work reported in this paper.

References

1. M.-H. Tsai and J.-W. Yeh, High-Entropy Alloys: A Critical Review, *Mater. Res. Lett.*, 2014, **2**, p 107–123. <https://doi.org/10.1080/21663831.2014.912690>
2. J.W. Yeh, S.K. Chen, S.J. Lin, J.Y. Gan, T.S. Chin, T.T. Shun, C.H. Tsau, and S.Y. Chang, Nanostructured High-Entropy Alloys with Multiple Principal Elements: Novel Alloy Design Concepts and Outcomes, *Adv. Eng. Mater.*, 2004, **6**, p 299–303. <https://doi.org/10.1002/adem.200300567>
3. B. Cantor, I.T.H. Chang, P. Knight, and A.J.B. Vincent, Microstructural Development in Equiatomic Multicomponent Alloys, *Mater. Sci. Eng. A*, 2004 <https://doi.org/10.1016/j.msea.2003.10.257>
4. L. Hou, J. Hui, Y. Yao, J. Chen, and J. Liu, Effects of Boron Content on Microstructure and Mechanical Properties of AlFeCoNiBx High Entropy Alloy Prepared by Vacuum Arc Melting, *Vacuum*, 2019, **164**, p 212–218. <https://doi.org/10.1016/j.vacuum.2019.03.019>
5. T. Yang, Y.L. Zhao, Y. Tong, Z.B. Jiao, J. Wei, J.X. Cai, X.D. Han, D. Chen, A. Hu, J.J. Kai, K. Lu, Y. Liu, and C.T. Liu, Multicomponent Intermetallic Nanoparticles and Superb Mechanical Behaviors of Complex Alloys, *Science*, 2018, **362**, p 933–937. <https://doi.org/10.1126/science.aas8815>
6. Z. Xu, D.Y. Li, and D.L. Chen, Effect of Ti on the Wear Behavior of AlCoCrFeNi High-Entropy Alloy During Unidirectional and Bi-Directional Sliding Wear Processes, *Wear*, 2021 <https://doi.org/10.1016/j.wear.2021.203650>
7. M. Pole, M. Sadeghilaridjani, J. Shittu, A. Ayyagari, and S. Mukherjee, High Temperature Wear Behavior of Refractory High Entropy Alloys Based on 4-5-6 Elemental Palette, *J. Alloys Compd.*, 2020 <https://doi.org/10.1016/j.jallcom.2020.156004>
8. R. Zhou, G. Chen, B. Liu, J. Wang, L. Han, and Y. Liu, Microstructures and Wear Behaviour of (FeCoCrNi)_{1-x}(WC)_x High Entropy Alloy Composites, *Int. J. Refract. Metal Hard Mater.*, 2018, **75**, p 56–62. <https://doi.org/10.1016/j.ijrmhm.2018.03.019>
9. P. Muangtong, A. Rodchanarowan, D. Chaysuwan, N. Chanlek, and R. Goodall, The Corrosion Behaviour of CoCrFeNi-x (x = Cu, Al, Sn) High Entropy Alloy Systems in Chloride Solution, *Corros. Sci.*, 2020 <https://doi.org/10.1016/j.corsci.2020.108740>
10. Y.Y. Liu, Z. Chen, J.C. Shi, Z.Y. Wang, and J.Y. Zhang, The Effect of Al Content on Microstructures and Comprehensive Properties in AlxCoCrCuFeNi High Entropy Alloys, *Vacuum*, 2019, **161**, p 143–149. <https://doi.org/10.1016/j.vacuum.2018.12.009>
11. S.E. Sünbül, K. İçin, F.Z. Şeren, Ö. Şahin, D.D. Cakil, R. Sezer, and S. Öztürk, Determination of Structural, Tribological, Isothermal Oxidation and Corrosion Properties of Al–Co–Cr–Fe–Ni–Ti–Cu High-Entropy Alloy, *Vacuum*, 2021, **187**, p 110072. <https://doi.org/10.1016/j.vacuum.2021.110072>
12. R. Gawel, Ł. Rogal, J. Dąbek, M. Wójcik-Bania, and K. Przybylski, High Temperature Oxidation Behaviour of Non-Equiatomic AlCoCrFeNi High Entropy Alloys, *Vacuum*, 2021 <https://doi.org/10.1016/j.vacuum.2020.109969>
13. S. Wang, Z. Chen, P. Zhang, K. Zhang, C.L. Chen, and B.L. Shen, Influence of Al Content on High Temperature Oxidation Behavior of AlxCoCrFeNiTi_{0.5} High Entropy Alloys, *Vacuum*, 2019, **163**, p 263–268. <https://doi.org/10.1016/j.vacuum.2019.01.053>
14. M. Lobel, T. Lindner, T. Mehner, and T. Lampke, Influence of Titanium on Microstructure, Phase Formation and Wear Behaviour of AlCoCrFeNiTi(x) High-Entropy Alloy, *Entropy*, 2018 <https://doi.org/10.3390/e20070505>
15. D. Kong, J. Guo, R. Liu, X. Zhang, Y. Song, Z. Li, F. Guo, X. Xing, Y. Xu, and W. Wang, Effect of Remelting and Annealing on the Wear Resistance of AlCoCrFeNiTi_{0.5} High Entropy Alloys, *Intermetallics*, 2019 <https://doi.org/10.1016/j.intermet.2019.106560>
16. Y.J. Zhou, Y. Zhang, Y.L. Wang, and G.L. Chen, Solid Solution Alloys of AlCoCrFeNiTi_x with Excellent Room-Temperature Mechanical Properties, *Appl. Phys. Lett.*, 2007 <https://doi.org/10.1063/1.2734517>
17. Y.J. Zhou, Y. Zhang, and Y.L. Wang, Solid Solution Alloys of AlCoCrFeNiTi_x with Excellent Room-Temperature Mechanical Properties, *Appl. Phys. Lett.*, 2007, **90**, p 181904.
18. X. Zeng, Z. Liu, G. Wu, X. Tong, Y. Xiong, X. Cheng, X. Wang, and T. Yamaguchi, Microstructure and High-Temperature Properties of Laser Cladded AlCoCrFeNiTi_{0.5} High-Entropy Coating on Ti 6Al-4V Alloy, *Surf. Coat. Technol.*, 2021 <https://doi.org/10.1016/j.surfcoat.2021.127243>
19. W.Y. Cui, W. Li, W.T. Chen, and F. Liou, Laser Metal Deposition of an AlCoCrFeNiTi_{0.5} High-Entropy Alloy Coating on a Ti6Al4V Substrate, *Microstruct. Oxidat. Behav. Cryst.*, 2020, **10**, p 638.
20. Y.J. Zhou, Y. Zhang, T.N. Kim, and G.L. Chen, Microstructure Characterizations and Strengthening Mechanism of Multi-Principal Component AlCoCrFeNiTi_{0.5} Solid Solution Alloy with Excellent Mechanical Properties, *Mater. Lett.*, 2008, **62**, p 2673–2676. <https://doi.org/10.1016/j.matlet.2008.01.011>
21. G. Liu, C. Xu, H. Chen, X. Hou, and Y. Liu, Electroless Deposition Method for Silver-Coated Carbon Fibres, *Micro Nano Lett.*, 2015, **10**, p 315–317. <https://doi.org/10.1049/mnl.2014.0620>
22. G. Zhao, Y. Zou, H. Zhang, and Z. Zou, Correlation Between Corrosion Resistance and the Local Atomic Structure of Electroless, Annealed Ni–P Amorphous Alloys, *Mater. Lett.*, 2014, **132**, p 221–223. <https://doi.org/10.1016/j.matlet.2014.06.081>
23. H. Luo, Q. Cai, B. Wei, B. Yu, D. Li, J. He, and Z. Liu, Effect of (NaPO₃)₆ Concentrations on Corrosion Resistance of Plasma Electrolytic Oxidation Coatings Formed on AZ91D Magnesium Alloy, *J. Alloy. Compd.*, 2008, **464**, p 537–543. <https://doi.org/10.1016/j.jallcom.2007.10.072>

24. A. Anupam, R.S. Kottada, S. Kashyap, A. Meghwal, B.S. Murty, C.C. Berndt, and A.S.M. Ang, Understanding the Microstructural Evolution of High Entropy Alloy Coatings Manufactured by Atmospheric Plasma Spray Processing, *Appl. Surf. Sci.*, 2020 <https://doi.org/10.1016/j.apsusc.2019.144117>
25. W. Wang, W. Qi, L. Xie, X. Yang, J. Li, and Y. Zhang, Microstructure and Corrosion Behavior of (CoCrFeNi)(95)Nb(5) High-Entropy Alloy Coating Fabricated by Plasma Spraying, *Materials*, 2019 <https://doi.org/10.3390/ma12050694>
26. M. Srivastava, M. Jadhav, R.P.S. Chakradhar, M. Muniprakash, and S. Singh, Synthesis and Properties of High Velocity Oxy-Fuel Sprayed FeCoCrNi2Al High Entropy Alloy Coating, *Surf. Coat. Technol.*, 2019 <https://doi.org/10.1016/j.surfcoat.2019.124950>
27. L. Chen, Y. Wang, X. Hao, X. Zhang, and H. Liu, Lightweight Refractory High Entropy Alloy Coating by Laser Cladding on Ti–6Al–4V Surface, *Vacuum*, 2021 <https://doi.org/10.1016/j.vacuum.2020.109823>
28. Y. Cui, J. Shen, S.M. Manladan, K. Geng, and S. Hu, Wear Resistance of FeCoCrNiMnAlx High-Entropy Alloy Coatings at High Temperature, *Appl. Surf. Sci.*, 2020 <https://doi.org/10.1016/j.apsusc.2020.145736>
29. J. Cheng, B. Sun, Y. Ge, X. Hu, L. Zhang, X. Liang, and X. Zhang, Nb Doping in Laser-cladded Fe25Co25Ni25(B0.7Si0.3)25 High Entropy Alloy Coatings: Microstructure Evolution and Wear Behavior, *Surf. Coat. Technol.*, 2020 <https://doi.org/10.1016/j.surfcoat.2020.126321>
30. G.H. Meng, N.A. Protasova, E.P. Kruglov, X. Lin, H. Xie, and X. Ding, Solidification Behavior and Morphological Evolution in Laser Surface Forming of AlCoCrCuFeNi Multi-Layer High-Entropy Alloy Coatings on AZ91D, *J. Alloy. Compd.*, 2019, **772**, p 994–1002. <https://doi.org/10.1016/j.jallcom.2018.09.120>
31. Q. Fan, C. Chen, C. Fan, Z. Liu, X. Cai, S. Lin, and C. Yang, Ultrasonic Suppression of Element Segregation in Gas Tungsten Arc Cladding AlCoCuFeNi High-Entropy Alloy Coatings, *Surf. Coat. Technol.*, 2021 <https://doi.org/10.1016/j.surfcoat.2021.127364>
32. Q. Fan, C. Chen, C. Fan, Z. Liu, X. Cai, S. Lin, and C. Yang, Effect of High Fe Content on the Microstructure, Mechanical and Corrosion Properties of AlCoCrFeNi High-Entropy Alloy Coatings Prepared by Gas Tungsten Arc Cladding, *Surf. Coat. Technol.*, 2021 <https://doi.org/10.1016/j.surfcoat.2021.127242>
33. G. Dai, S. Wu, and X. Huang, Preparation Process for High-Entropy Alloy Coatings based on Electroless Plating and Thermal Diffusion, *J. Alloy. Compd.*, 2022 <https://doi.org/10.1016/j.jallcom.2022.163736>
34. A. Vallimanan, S.P.K. Babu, S. Muthukumar, M. Murali, V. Gaurav, and R. Mahendran, Corrosion Behaviour of Thermally Sprayed Mo Added AlCoCrNi High Entropy Alloy Coating, *Mater. Today Proc.*, 2020, **27**, p 2398–2400. <https://doi.org/10.1016/j.matpr.2019.09.149>
35. S. Li and T. Yamaguchi, High-Temperature Oxidation Performance of Laser-Cladded Amorphous TiNiSiCrCoAl High-Entropy Alloy Coating on Ti-6Al-4V Surface, *Surf. Coat. Technol.*, 2022 <https://doi.org/10.1016/j.surfcoat.2022.128123>
36. H. Liu, Q. Gao, J. Dai, P. Chen, W. Gao, J. Hao, and H. Yang, Microstructure and High-Temperature Wear Behavior of CoCrFeNiWx High-Entropy Alloy Coatings Fabricated by Laser Cladding, *Tribol. Int.*, 2022 <https://doi.org/10.1016/j.triboint.2022.107574>
37. X.W. Tao, Z.J. Yao, S.S. Zhang, J. Liao, and J. Liang, Investigation on Microstructure, Mechanical and Tribological Properties of In-Situ (TiB + TiC)/Ti Composite During the Electron Beam Surface Melting, *Surf. Coat. Technol.*, 2018, **337**, p 418–425. <https://doi.org/10.1016/j.surfcoat.2018.01.054>
38. O.B. Perevalova, A.V. Panin, and M.S. Kazachenok, Concentration-Dependent Transformation Plasticity Effect During Hydrogenation of Technically Pure Titanium Irradiated with an Electron Beam, *Russ. Phys. J.*, 2019, **61**, p 1992–2000. <https://doi.org/10.1007/s11182-019-01629-8>
39. T. Yu, H. Wang, K. Han, and B. Zhang, Microstructure and Wear Behavior of AlCrTiNbMo High-Entropy Alloy Coating Prepared by Electron Beam Cladding on Ti600 Substrate, *Vacuum*, 2022 <https://doi.org/10.1016/j.vacuum.2022.110928>
40. T. Yu, H. Wang, K. Han, Y. Wang, Y. Qiu, and B. Zhang, Mo20Nb20Co20Cr20(Ti8Al8Si4) Refractory High-Entropy Alloy Coatings Fabricated by Electron Beam Cladding: Microstructure and Wear Resistance, *Intermetallics*, 2022 <https://doi.org/10.1016/j.intermet.2022.107669>
41. A.A. Ruktuev, D.V. Lazurenko, T.S. Ogneva, R.I. Kuzmin, M.G. Golkovski, and I.A. Bataev, Structure and Oxidation Behavior of CoCrFeNiX (where X is Al, Cu, or Mn) Coatings Obtained by Electron Beam Cladding in Air Atmosphere, *Surf. Coat. Technol.*, 2022 <https://doi.org/10.1016/j.surfcoat.2022.128921>
42. I.A. Bataev, D.O. Mul, A.A. Bataev, O.G. Lenitseva, M.G. Golkovski, Y.S. Lizunkova, and R.A. Dostovalov, Structure and Tribological Properties of Steel After Non-Vacuum Electron Beam Cladding of Ti, Mo and Graphite Powders, *Mater. Charact.*, 2016, **112**, p 60–67. <https://doi.org/10.1016/j.matchar.2015.11.028>
43. S. Guo, Q. Hu, C. Ng, and C.T. Liu, More than Entropy in High-Entropy Alloys: Forming Solid Solutions or Amorphous Phase, *Intermetallics*, 2013, **41**, p 96–103. <https://doi.org/10.1016/j.intermet.2013.05.002>
44. V. Shivam, Y. Shadangi, J. Basu, and N.K. Mukhopadhyay, Alloying Behavior and Thermal Stability of Mechanically Alloyed Nano AlCoCrFeNiTi High-Entropy Alloy, *J. Mater. Res.*, 2019, **34**, p 787–795. <https://doi.org/10.1557/jmr.2019.5>
45. Z. Xiong, S. Liu, X. Wang, C. Shang, X. Li, and R.D.K. Misra, The Contribution of Intragranular Acicular Ferrite Microstructural Constituent on Impact Toughness and Impeding Crack Initiation and Propagation in the Heat-Affected Zone (HAZ) of Low-Carbon Steels, *Mater. Sci. Eng., A*, 2015, **636**, p 117–123. <https://doi.org/10.1016/j.msea.2015.03.090>
46. Y. Cai, L. Zhu, Y. Cui, M. Shan, H. Li, Y. Xin, and J. Han, Fracture and Wear Mechanisms of FeMnCrNiCo+x(TiC) Composite High-Entropy Alloy Cladding Layers, *Appl. Surf. Sci.*, 2021 <https://doi.org/10.1016/j.apsusc.2020.148794>
47. B. Bax, M. Schäfer, C. Pauly, and F. Mücklich, Coating and Prototyping of Single-Phase Iron Aluminide by Laser Cladding, *Surf. Coat. Technol.*, 2013, **235**, p 773–777. <https://doi.org/10.1016/j.surfcoat.2013.09.001>

Publisher's Note Springer Nature remains neutral with regard to jurisdictional claims in published maps and institutional affiliations.

Springer Nature or its licensor (e.g. a society or other partner) holds exclusive rights to this article under a publishing agreement with the author(s) or other rightsholder(s); author self-archiving of the accepted manuscript version of this article is solely governed by the terms of such publishing agreement and applicable law.